A double-stranded DNA rotaxane

Damian Ackermann[1], Thorsten L. Schmidt[2], Jeffrey S. Hannam[1], Chandra S. Purohit[1], Alexander Heckel[2] and Michael Famulok[1]*

Mechanically interlocked molecules such as rotaxanes and catenanes have potential as components of molecular machinery. Rotaxanes consist of a dumb-bell-shaped molecule encircled by a macrocycle that can move unhindered along the axle, trapped by bulky stoppers. Previously, rotaxanes have been made from a variety of molecules, but not from DNA. Here, we report the design, assembly and characterization of rotaxanes in which both the dumb-bell-shaped molecule and the macrocycle are made of double-stranded DNA, and in which the axle of the dumb-bell is threaded through the macrocycle by base pairing. The assembly involves the formation of pseudorotaxanes, in which the macrocycle and the axle are locked together by hybridization. Ligation of stopper modules to the axle leads to the characteristic dumb-bell topology. When an oligonucleotide is added to release the macrocycle from the axle, the pseudorotaxanes are either converted to mechanically stable rotaxanes, or they disassemble by means of a slippage mechanism to yield a dumb-bell and a free macrocycle. Our DNA rotaxanes allow the fields of mechanically interlocked molecules and DNA nanotechnology to be combined, thus opening new possibilities for research into molecular machines and synthetic biology.

Rotaxanes are a class of mechanically interlocked molecules consisting of at least one macrocycle threaded over a dumb-bell-shaped molecule, in which the macrocycle is kinetically trapped by rigid and bulky stoppers[1,2]. These molecules have attracted much attention as functional materials, and the so-called mechanical bond[3] is the *de facto* reason for the legion of examples describing the enhanced physical properties of rotaxanes when compared with their non-interlocked components, including enzymatic protection[4], dye fluorescence[5] and electroluminescence[6]. One of the most striking features of rotaxane architectures is that their mechanically interlocked components can move relative to one another with large-amplitude motions, which has use in prototypical design features of components for nanoscale machinery[7]. In the field of organic chemistry, a number of classical supramolecular cognate motifs exist as interlocking models, which have applications in constructing molecular architectures[8] that can be used to control sub-molecular motion through the application of external stimuli[9]. Indeed, under the influence of such external stimuli the movement of components can be used to vary physical properties such as conductivity[10], fluorescence[11], porosity[12] and wettability[13].

Methods of extending these approaches to DNA-based nano-devices are unprecedented, but highly desirable, owing to the superiority of DNA over other construction materials. DNA is an ideal material for the bottom-up fabrication of nanometre-scale objects and nanomechanical devices because of the reliable interactions that bind complementary oligonucleotides together in a double helix[14–16]. Furthermore, DNA has a combination of properties that are a prerequisite for building more competent nanomechanical devices based on the high information density of DNA (one bit comprised of one base pair occupies a volume of $\sim$1 nm^3), the principal ability to evolve, its simplicity, and the fact that it can easily be functionalized with an array of chemical groups. Indeed, DNA nanotechnology has furnished the scientific world with a plethora of topologies in the form of designed patterns[17], algorithmically ordered arrays[18,19], logic gates[20,21] and geometries in both the second[22] and third dimensions[23]. Additionally, the programmable aspect[24] of DNA enables facile post-assembly modification of

fabricated constructs in response to external applied stimuli[25,26]. Some of these designed systems allow repetitive, processive steps characteristic of bipedal molecular motors and switches that emulate certain biological motor proteins[27–30]. Rotaxanes made of double-stranded DNA (dsDNA) with mobile interlocked components would be attractive devices for use in nanorobotics, because they have a unique mechanical bonding motif, not available to conventional building blocks. Simple interlocked structures made of single-stranded (ss) circular DNAs have been described, but these systems are immobile, because of the different stabilizing interactions such as double- and triple-strand formation or other tertiary interactions that ssDNAs assume with the interlocked partner[31,32].

Recently, we described the efficient synthesis of DNA mini-circles containing bespoke gap regions, which could be used as handles for the construction of higher-order nano-objects[33–35]. The DNA circles show hardly any ring strain because they contain repetitive, intrinsically bent AT-tracts that cooperatively result in the circular shape of the double helix with 105, 126, 147, 168 or more base pairs (bp)[36]. In the initial conception of this described research, we reasoned that the combination of the different properties of rotaxane architectures, such as mechanical interlocking and facility of construction, and those of DNA as a carrier of information, could potentially lead to an exciting hybrid structure of DNA rotaxanes.

Interlocking principle and assembly of pseudorotaxanes

The interlocking approach used here involves the synthesis of pseudorotaxane species as a prerequisite for the assembly of a DNA–rotaxane. To assemble a DNA–pseudorotaxane, a linear DNA rod was threaded through a dsDNA ring containing a single-strand gap of 13 nucleotides (Supplementary Figs S1,S2). As the DNA rod itself contained an 8-mer complementary single-strand region covering more than half but less than one helical turn, threading of the DNA rod occurred as a consequence of hybridization to the gap-ring (Fig. 1a, Supplementary Fig. S3). The size of the stoppers had to be at least as large as the inner diameter of a 168-bp gap-ring, which is $\sim$14–15 nm (ref. 34). This size is much larger than the

[1]LIMES Institute, Program Unit Chemical Biology & Medicinal Chemistry, c/o Kekulé Institut für Organische Chemie und Biochemie, University of Bonn, Gerhard-Domagk-Straße 1, 53121 Bonn, Germany, [2]University of Frankfurt, Cluster of Excellence Macromolecular Complexes, Max-von-Laue-Str. 9, 60438 Frankfurt, Germany. *e-mail: m.famulok@uni-bonn.de
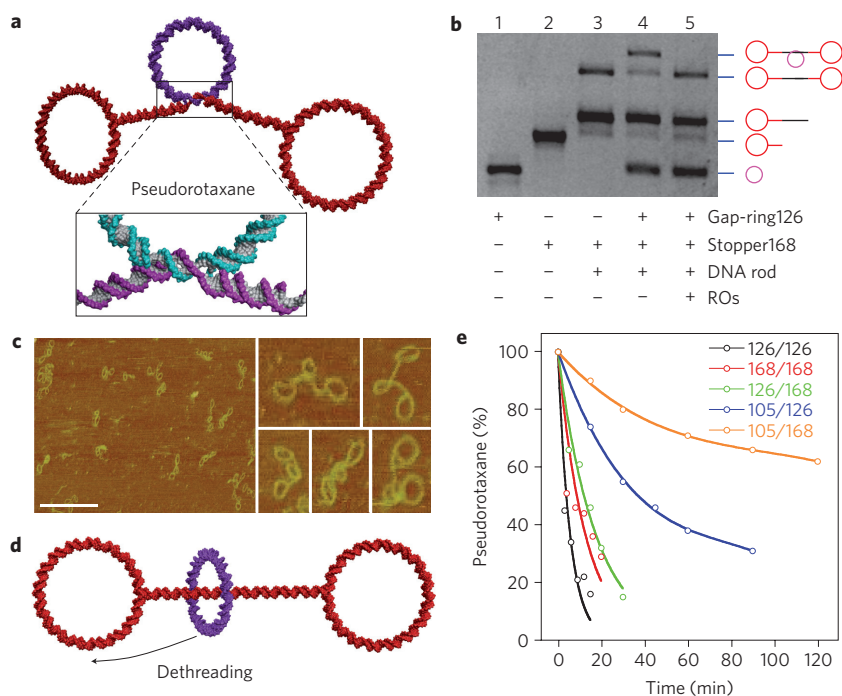
Figure 1 | Architecture of DNA–pseudorotaxanes with single-ring stoppers. a, Molecular model of a pseudorotaxane composed of a 126-bp macrocycle with a 13-mer single-stranded gap hybridized to a 8-mer single-stranded region in the axle. The box shows the single-stranded part of the threaded DNA rod hybridized to the gap. **b**, Analytical agarose gel (2%) of 126/168-rotaxane synthesis. Lane 1, gap-ring126; lane 2, stopper168; lane 3, products of the ligation of the DNA rod and stopper168; lane 4, products of the ligation of the DNA rod with the threaded gap-ring126, and stopper168; lane 5, as in lane 4, with subsequent addition of ROs. The pseudorotaxane completely disappears due to dethreading of the macrocycle. **c**, AFM scans of the purified upper band in lane 4 of the gel shown in **b** adsorbed on polyornithine-coated mica surfaces confirm the pseudorotaxane structure. In the enlarged sections, the threaded ring is clearly visible to be smaller than the flanking stopper rings (right panels). Scale bar, left AFM image, 250 nm. **d**, Molecular model of short-lived rotaxane intermediate obtained in the presence of the ROs. **e**, Time-dependent pseudorotaxane disassembly triggered by the 13-mer RO 105-insert. The graph shows the fraction of remaining pseudorotaxane calculated from band intensities of analytical agarose gels (Supplementary Fig. S5) of various single-ring-stoppered rotaxanes. Curve fits represent trend lines. The nomenclature of the various species refers to the number of base pairs in the macrocycle and in the stopper.

diameter of any single protein (for comparison: the diameter of a ribosome is ∼18–20 nm; ref. 37). Therefore, in a first version, 168-bp single rings were used as stoppers (Supplementary Fig. S3). They were ligated onto each side of the rod, resulting either in a dumb-bell-shaped DNA object or, in the presence of a 126-bp gap-ring, in a dsDNA–pseudorotaxane (Supplementary Figs S1–S3). The integrity of both the dumb-bell and the pseudorotaxane were confirmed by gel electrophoresis and atomic force microscopy (AFM; Fig. 1b,c and Supplementary Fig. S4). These data displayed the planar nature of the flanking stoppers, and the presence of the DNA macrocycle. We found all pseudorotaxanes obtained in this way to remain stable indefinitely under standard buffer conditions. After consecutive ligation of the 13-mer and the 8-mer release oligonucleotides (ROs), which are complementary to the single-stranded regions of the gap-ring and the DNA rod, respectively, the pseudorotaxane was converted into a 'genuine' rotaxane having the ability for free translational motion along the axle. According to gel-shift experiments (Fig. 1b), however, the rotaxane only exists as a short-lived intermediate, which rapidly disassembles into the free DNA macrocycle and the dumb-bell by means of dethreading (Fig. 1d). When a scrambled, non-complementary version of the RO was used as a negative control, the pseudorotaxane remained unaltered and the interlocked integrity was maintained (data not shown). Apparently, the ROs efficiently hybridize with their complementary counterparts, causing the detachment of the DNA macrocycle from the DNA rod in the pseudorotaxane. However, the 168-bp rings are not rigid enough to serve as efficient stoppers capable of trapping the DNA macrocycle within the dumb-bell, resulting in slippage of the macrocycle over the stopper rings. Nevertheless, this result also implies that the DNA macrocycle has free translational mobility along the vector of the DNA axle. The phenomenon of slippage has also been observed by organic chemists in hydrogen bond assembled rotaxanes, and has been elegantly used by Stoddart and colleagues for rotaxane synthesis[38].

Stability of rotaxanes

To investigate systematically the relationship between slippage and ring size, we determined the lifetime of a set of pseudorotaxanes assembled by using any combination of different DNA gap-rings and single-ring stoppers having 105, 126 and 168 bp, respectively. Dethreading of the rotaxanes was quantified by integration of the band intensities of pseudorotaxane and dumb-bell from gel-shift experiments (Supplementary Fig. 5). By plotting the relative fraction of the remaining rotaxane versus time, disassembly curves were obtained (Fig. 1e), and lifetimes were empirically determined. The RO-triggered pseudorotaxane disassembly occurred within 15–25 min, when the macrocycle and the stoppers were of the same size, as in the 168/168- and 126/126-rotaxanes, respectively. Reducing the size of the DNA macrocycles versus the stoppers increased the lifetime to ∼30 min in the 126/168-system, to >100 min in the 105/126-system, and to ≫180 min in the combination of the 105-bp macrocycle with the 168-bp stoppers, showing that these pseudorotaxanes dethread considerably more slowly. Thus, the pseudorotaxanes, although highly stable in the absence of the cognate RO, disassemble within hours to form
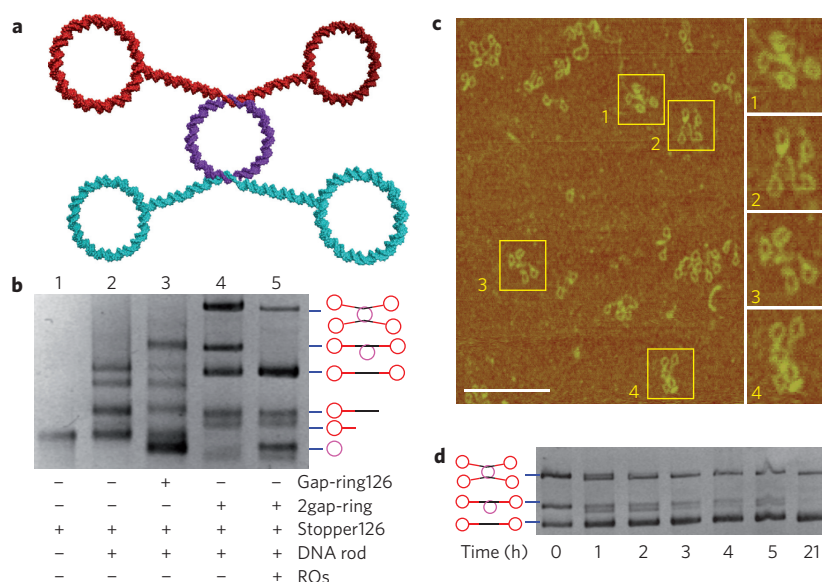
Figure 2 | Architecture of a DNA pseudo[3]rotaxane. a, Molecular model of the pseudo[3]rotaxane. **b**, Analytical agarose gel (2%) of pseudo[3]rotaxane synthesis. Lane 1, stopper126; lane 2, products of ligation of the DNA rod and stopper126; lane 3, products of ligation of the DNA rod with a threaded one-gap-ring126, and stopper126; lane 4, products of ligation of the DNA rod with a threaded two-gap-ring126, and stopper126; lane 5, as in lane 4, in the presence of an excess of the RO 105-insert after 48 h. The RO was added at 4 °C and left at this temperature for 20 min. Compared to lane 4, the bands corresponding to the free dumb-bell and the free DNA macrocycle have clearly increased, indicating that dethreading has occurred. The top band in lane 4 was purified by weak anion exchange chromatography and used for AFM studies. **c**, AFM images of the purified top band from lane 4 of the gel shown in **b** confirm the pseudo[3]rotaxane structure. At higher magnifications the threaded ring is clearly visible (numbers correspond to the species in the main panel). Scale bar (main panel), 200 nm. **d**, Pseudo[3]rotaxane disassembly triggered by the 13-mer RO 105-insert. The analytical agarose gel shows the conversion from pseudo[3]rotaxane to dumb-bell at the indicated time points. The intermediary-formed pseudo[2]rotaxane disassembles more quickly than the pseudo[3]rotaxane.

the dumb-bell and the free macrocycle in its presence. Taken together, these results show a clear correlation between the relative sizes of both the stoppers and the macrocycles with dethreading time, similar to the behaviour of small-molecule organic rotaxanes[39].

Multiple threading

We next constructed a 126-bp DNA macrocycle with two opposing 13-nucleotide gap regions of identical sequence (Supplementary Fig. S2d) to extend the assembly process to multiple threading. Although the repetitive AT-tracts in this ring were interrupted by two straight sequences, the remaining AT-tracts still showed sufficient curvature to allow cooperative ring formation. This design enables the preparation of significantly more complex architectures such as a [3]rotaxane with two thread molecules circumscribed by a 126-bp DNA macrocycle (Fig. 2a and Supplementary Figs S6,S7). Starting from the two-gap-ring, the threading of two rods, followed by the ligation of the 126-bp stoppers, led to the pseudo[3]rotaxane (Fig. 2b, lane 4). This species was purified, and its integrity was verified by AFM (Fig. 2c). The AFM image clearly shows the presence of the four thread rings and the macrocycle in the majority of the visible structures. At 4 °C, in the presence of RO, the pseudo[3]rotaxane disassembled to the dumb-bell and the free macrocycle within ~48 h (Fig. 2b, lane 5, Fig. 2d). The more rapid disappearance of the intermediary-formed pseudo[2]rotaxane is consistent with the previously tested 126/126-system. Although this type of [3]rotaxane displays dethreading behaviour, the ability to assemble multiply threaded architectures of this type is exciting as it opens up, in principle, the possibility of expanding these systems to [4]-, [5]- and even higher-order DNA–rotaxanes, with increasing numbers of macrocycles threaded over one or two axles, simply by choosing different two-gap-rings and by extending the axles to include the respective complementary hybridization sites.

Mechanically stable dsDNA rotaxane

To obtain mechanically stable rotaxanes, we assembled stopper modules with a spherical geometry in a new sub-architecture consisting of two crossover rings (Fig. 3a and Supplementary Fig. S8). These intertwined crossover rings are more bulky than single rings. When used as stoppers, they should prevent dethreading of the macrocycle, resulting in a genuinely interlocked rotaxane with the topology and dimensions shown in the molecular model (Fig. 3a). The design of the crossover rings is based on the 'AT-tract model' of two 168-bp DNA minicircles, which are connected through Holliday junctions at the poles (Fig. 3b and Supplementary Fig. S9a,b). Note, however, that the model shown displays the topology of the spherical stopper modules in an idealized geometry, because Holliday junctions are known to assume a stacked X-conformation with a torsion angle of ~60° (refs 40,41), but ~40° angles are also known from crystal structures[42] and AFM studies[43]. Because the structure of the crossover rings is not known, the Holliday junctions in the molecular model of the DNA–rotaxane (Fig. 3a) are drawn with a torsion angle of 90° for clarity and to illustrate the topology. The basic shape of the spherical stopper modules is reminiscent of the recently described spherical wireframe capsules[44], although they significantly differ in their skeletal structure, size and complexity.

As with the single-ring stoppers, a short DNA duplex with a sticky end for subsequent ligation is attached to the equator of the sphere by means of a three-way junction (Supplementary Figs S8a,S9b). These spherical stoppers were assembled from 15 individual oligonucleotides in three steps via quarter and hemisphere intermediates (Fig. 3b and Supplementary Fig. S9c, Supplementary Movie S1). Although the quarter sphere was used without purification, it was essential to purify the hemisphere and the spherical stoppers by weak anion exchange column chromatography (Supplementary Methods, Supplementary Fig. S10). The pseudorotaxanes were
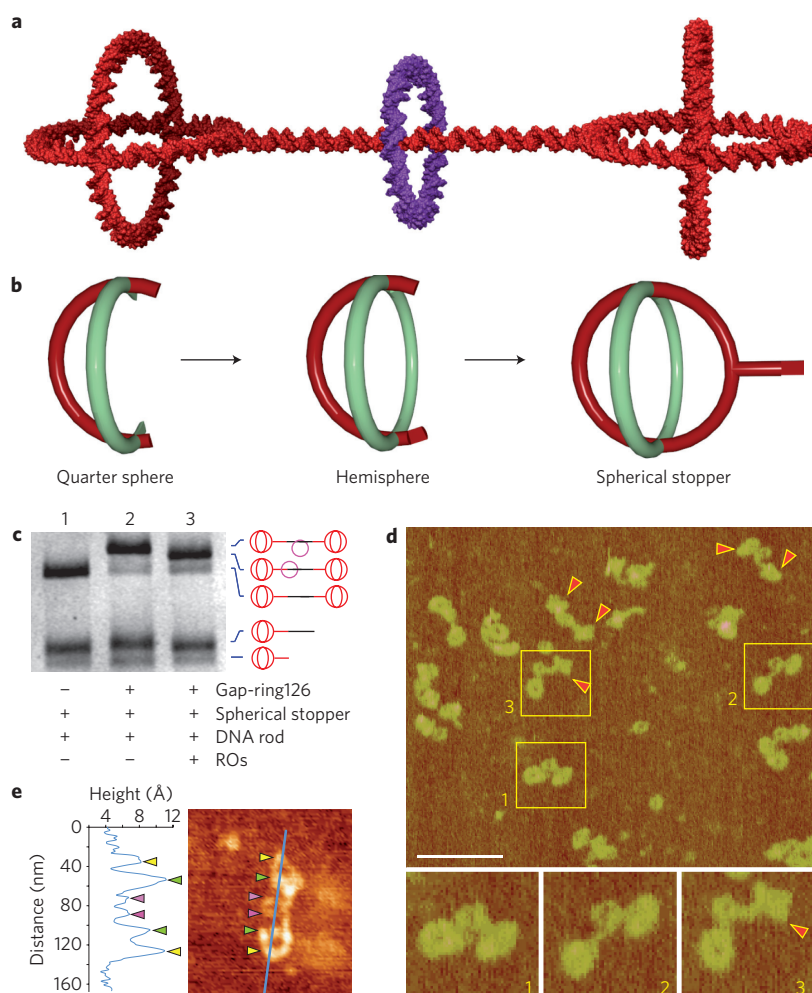
Figure 3 | Architecture of DNA–rotaxanes with spherical stoppers. a, Molecular model of a DNA–rotaxane assembled from 168-bp spherical stoppers and a 126-bp DNA macrocycle. Holliday junctions are drawn in an idealized geometry with a torsion angle of 90°, because the structure of the crossover rings is unknown. **b**, Stepwise assembly of the spherical stoppers via a quarter sphere and hemisphere. **c**, Analytical agarose gel (2%) of the 126/168 spherical-stopper rotaxane synthesis. Lane 1, products of ligation of the DNA rod and spherical stopper168 (dumb-bell); lane 2, products of ligation of the DNA rod with the threaded gap-ring126, and spherical stopper168 (pseudorotaxane); lane 3, unpurified pseudorotaxane incubated with RO. Despite the slightly increased charge and molecular weight resulting from the added ROs, the new band that appears migrates more quickly than the pseudorotaxane and is clearly distinct from the dumb-bell. The product that appeared in lane 3 was purified by weak anion exchange chromatography and used for AFM studies. **d**, AFM images of the purified upper band in lane 3 of the gel in **c** confirm the rotaxane structure. Arrows indicate the crossover structure of the stopper rings. At higher magnifications, the threaded ring is clearly smaller than the flanking stopper rings (lower panels: numbers correspond to the species in the top panel). Scale bar (main AFM image), 130 nm. **e**, Quantitative height analysis of a genuine spherical-stopper rotaxane shows that the height of the spherical stoppers (green and yellow arrowheads) significantly exceeds that of the threaded macrocycle (pink arrowheads).

assembled analogously to those prepared previously (Supplementary Fig. 8b). Figure 3c shows that nearly quantitative threading was achieved in the presence of two equivalents of gap-ring126, whereas the dumb-bell, which is formed from a residual unthreaded DNA rod, appears as a faint band only (Fig. 3c, lane 2). After adding the ROs, the pseudorotaxane completely merged into a new product of slightly faster mobility than the pseudorotaxane (Fig. 3c, lane 3). This product remained unchanged for at least 7 days at 4 °C (Supplementary Fig. S11); also, over 72 h at room temperature, no dethreading was observed at all.

Analysis of the purified product by AFM confirmed the topology of a DNA–rotaxane in which a smaller macrocycle is interlocked with a dumb-bell-shaped object (Fig. 3d), with the expected length of ~70 nm. Supplementary Fig. S12 directly compares the AFM scans of the genuine DNA–rotaxanes containing spherical stoppers with pseudorotaxanes containing single-ring stoppers. The colour code reflecting the height of the objects permits discrimination between simple DNA rings and spherical objects. The pseudorotaxanes do not exceed a height of 1 nm, consistent with their flat adsorption to the surface, whereas the spherical stoppers clearly exceed this height owing to their three-dimensional expansion from the surface. A quantitative AFM height analysis (Fig. 3e) revealed a significant difference in height between the interlocked DNA ring and the spherical stoppers, and again a clear difference in width.

We next sought to compare the relative stabilities of rotaxanes by varying the size and topology of the stoppers and the corresponding macrocycles. For this purpose we prepared pairs of pseudorotaxanes mechanically maintained by single-ring (168-bp) or spherical (168-bp) stoppers, respectively, threaded with 126-bp or 168-bp macrocycles, respectively. The pseudorotaxanes were incubated with ROs for 30 min at 4 °C and then analysed by gel electrophoresis (Fig. 4a). As expected, the bands corresponding to the pseudo-rotaxanes of the single-ring systems almost completely disappeared.
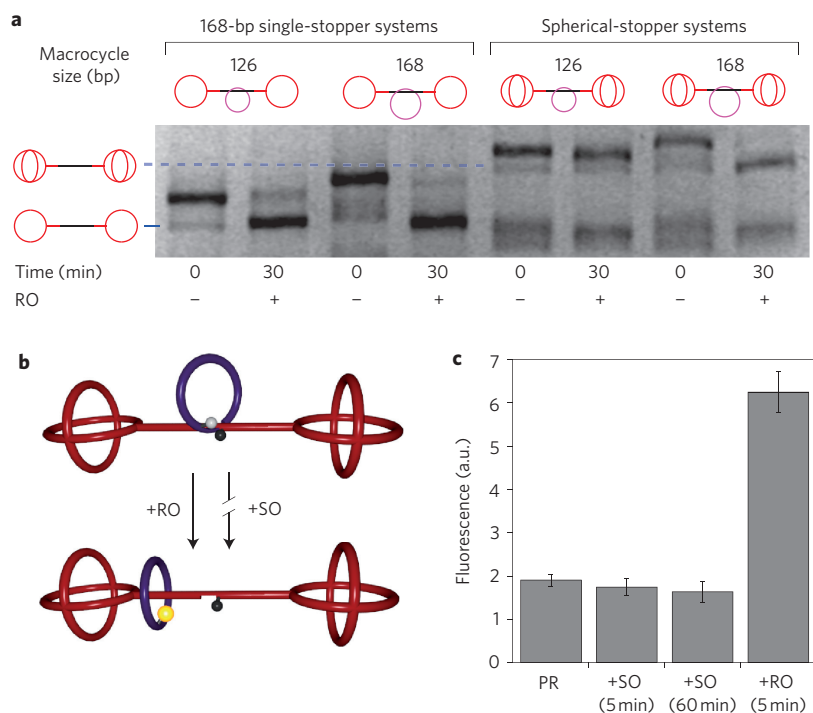
Figure 4 | Rotaxane stability and macrocycle mobility studies. a, Analytical agarose gel of macrocycle release, triggered by RO 105-insert. The first lane of each ring system investigated corresponds to the pseudorotaxane; the second lane corresponds to the product mixture analysed after 30 min of incubation with 105-insert at 4 °C. The pseudorotaxanes of both single-ring systems and of the spherical-ring system with a 168-bp threaded macrocycle are nearly completely converted to the corresponding dumb-bell after 30 min. In the case of the spherical-ring system with a 126-bp threaded macrocycle, no increase in the dumb-bell intensity can be observed. Again, the band of the main product (lane 6) is slightly shifted compared to the pseudorotaxane (lane 5), consistent with the formation of a new product. **b**, Triggered release of a fluorescently labelled macrocycle. The fluorescence of the Cy3 dye (white) attached to the macrocycle is quenched by the BHQ2-labelled axle (black) in the pseudorotaxane. When the macrocycle is released from the axle, fluorescence of Cy3 (yellow) is observed due to dequenching. This only occurs when the 13-mer oligonucleotide 105-insert (RO) is used but not the scrambled version (SO). **c**, Fluorescence of the pseudorotaxane was measured at 600 nm and remained unchanged for 5 and 60 min when treated with SO. Five minutes after addition of the RO 105-insert, the fluorescence intensity increased by a factor of three, demonstrating the free mobility of the macrocycle.

Interestingly, the spherical-ring system was unable to prevent the 168-bp macrocycle from dethreading, with nearly complete disassembly occurring within 30 min. In contrast, the 126-bp macrocycle displays absolutely no such disassembly. This result demonstrates that the rotaxane based on a 126-bp macrocycle and spherical stoppers made of 168-bp crossover rings remains mechanically stable, even after seven days. Intriguingly, we have demonstrated that the transition from unstable pseudorotaxane to fully stable rotaxane occurs over a relatively narrow change in the dimensions of the threaded macrocycle rings. Despite the flexibility of the DNA components that prevented the formation of stable rotaxanes in the initial studies, a stable rotaxane is formed at some cutoff point. An analogous phenomenon has also been observed in crown ether/ammonium ion rotaxane systems[45]. It is noteworthy that our results broadly agree with those observed in molecules that significantly differ in their size and composition from the DNA-based architectures described here.

To provide unambiguous evidence that the 126-bp macrocycle shows free mobility along the vector of the axle, we performed a fluorescence quenching experiment. Gap-ring126 was labelled with a Cy3 dye at the 5′-end of the gap and the quencher BHQ2 was attached at the 3′-position of the gap sequence of the axle (Supplementary Fig. S13). Thus, in the pseudorotaxane, the fluorescence of the Cy3-labelled gap-ring was quenched due to its hybridization with the axle gap, rendering both dyes in close proximity. Conversely, fluorescence emission occurred when the macrocycle was released from hybridization to its complementary sequence in the axle (Fig. 4b). Indeed, within 5 min after the

addition of the RO that was complementary to the gap sequence in the macrocycle, the fluorescence signal increased significantly from ~2 to ~6 arbitrary units. As a control we used a scrambled version of this oligonucleotide (SO) that was non-complementary to the gap sequence and thus could not release the macrocycle. At both time points, 5 min and 60 min after the addition of SO, the fluorescence emission was unchanged with respect to the pseudorotaxane (Fig. 4c). Taken together, these results clearly demonstrate that the macrocycle has translational motion that can be triggered in a highly specific fashion by a complementary RO within at least 5 min. This paves the way for switchable systems based on a dsDNA molecular shuttle.

Conclusions

We have reported a straightforward, reliable and modular threading method that provides access to a class of entirely double-stranded interlocked DNA nano-objects of circular geometry. The rotaxanes we obtained have the potential to be applied as versatile components in nanomechanics and nanorobotics. When using single rings as stopper modules, we encountered disassembly of the interlocked superstructure due to the inherent flexibility of the components. However, we broadly observed a correlation between size complementarity and dethreading time. This offers the exciting possibility of assembling more complex DNA architectures that show a function dependent on the mechanically fine-tuned sliding of the macrocycle. By using crossover DNA rings as stoppers, a stable rotaxane was obtained in which the dethreading of the DNA macrocycle was prevented. The modular nature and step-by-step assembly

could lead to the straightforward construction of multiply inter-locked rotaxane species. Furthermore, our DNA architectures are reminiscent of toroidal proteins that are threaded over DNA in a variety of biological systems that control DNA replication and degradation, or its packaging and transport. For example, DNA polymerases are anchored to sliding DNA clamps like the bacterial β clamp to prevent dissociation of the processive enzyme from the DNA substrate. DNA sliding clamps enable the polymerase to add thousands of bases in a few seconds without detaching from the template[46]. The DNA macrocycle interlocked with a linear DNA axle can be viewed as the synthetic DNA equivalent of these protein clamps. Thus, in principle, through chemical modification or covalent attachment of appropriate protein domains, processive catalytic systems that perform chemistry on the DNA templates onto which they are threaded could be accessible, opening up new opportunities in synthetic biology and nanorobotics.

Methods

DNA. The DNA sequences were ordered 5′-phosphorylated and purified by high-performance liquid chromatography (HPLC) from METABION. All DNA strands were verified by mass spectrometry (MS) analysis. The names and sequences of all the strands are given in Supplementary Table S1.

Buffer systems. 1 × TAE buffer: 40 mM Tris, 20 mM AcOH, 1 mM EDTA. 1 × DNA store buffer: 10 mM Tris·HCl, 50 mM NaCl, 10 mM MgCl$_2$ at pH 7.5.

HPLC purification. Weak anion exchange HPLC purification: column TSKgel DEAE-NPR 4,6 mm × 35 mm (TOSOH); buffer A: 20 mM Tris·HCl, pH 9.0; buffer B: buffer A + 1 M NaCl; gradient 40% → 65% B in 30 min. After purification, the product fractions were concentrated using Ultracel Centrifugal Filters (YM-30, YM-100, MILLIPORE), washed twice with 1 × DNA store buffer and eluted in 100 μl 1 × DNA store buffer.

Gel electrophoresis. Analytical polyacrylamide gels were run in 1 × TAE for 25 min at 200 V, stained with ethidium bromide and visualized under UV irradiation. Agarose gels were poured from 'Agarose High Resolution' (ROTH) in 0.5 × TAE and were run for 15–20 min at 200 V, stained with ethidium bromide and visualized under UV irradiation.

Synthesis of gap rings and single-ring stoppers. Oligonucleotides (800 pmol) and 40 mM NaCl in 1 × ligase buffer (200 μl) were annealed from 60 °C to 15 °C over 75 min ($\Delta T/\Delta t = -36$ °C h^{-1}). Ligase (2 μl, 10 U) was added and ligated over night at 15 °C. The ligation products were analysed by polyacrylamide gel electrophoresis (PAGE; 6% acrylamide in 1 × TAE). The products were purified by HPLC and concentrated using Ultracel YM-30 Centrifugal Filters.

Synthesis of spherical stoppers. Oligonucleotides (3.2 nmol) HJalpha b, HJalpha c, HJalpha d, HJbeta a, HJbeta kc, HJbeta kd, Bogen r, Bogen f, and 20 mM NaCl in 1 × ligase buffer (720 μl) were annealed from 60 °C to 15 °C over 75 min ($\Delta T/\Delta t = -36$ °C h^{-1}). Ligase (8 μl, 40 U) was added and ligated over night at 15 °C to give the quarter sphere as one uniform product (Supplementary Fig. S8a, lane 2). In another vial, 3.2 nmol oligonucleotides HJalpha a, Ring1 r, Ring1 f and 20 mM in 1 × ligase buffer (240 μl) were annealed from 60 °C to 15 °C over 75 min ($\Delta T/\Delta t = -36$ °C h^{-1}) and ligated for 30 min at 15 °C by adding 2 μl ligase (10 U). This pre-ligated sample was added to the quarter-sphere sample and ligation was continued for 6 h to give the hemisphere. The crude was analysed on a 6% PAGE (Supplementary Fig. S8a, lane 3), purified by weak anion exchange HPLC, concentrated using Ultracel YM-100 Centrifugal Filters. In a third vial, 200 pmol oligonucleotides HJbeta b, Ring2 r, RingSE a, RingSE b and 20 mM in 1 × ligase buffer (40 μl) were annealed from 60 °C to 15 °C over 75 min ($\Delta T/\Delta t = -36$ °C h^{-1}) and ligated for 30 min at 15 °C by adding 0.5 μl ligase (2.5 U). This pre-ligated sample was added to the hemisphere (200 pmol in 240 μl 1 × ligase buffer) and ligation was continued for 6 h to give the spherical stopper in a quantitative reaction. The crude of the spherical stopper was analysed on a 2% agarose gel (Supplementary Fig. S10b), purified by weak anion exchange HPLC, concentrated using Ultracel YM-100 Centrifugal Filters.

Rotaxane synthesis. The gap-ring (2 equiv.) and the DNA rod (1 equiv., a solution of EFCT-1/EFCT-2/EF3long 1:1:1 in 1 × DNA store buffer) were combined, diluted with H$_2$O to 22.5 μl, and 2.5 μl of 10 × ligase buffer was added. The solution was kept at room temperature overnight and then cooled to 15 °C for 1 h. A solution of 2.5 equiv. of stopper in 30 μl of 1 × ligase buffer was then added. After hybridizing for 30 min at 15 °C, 0.3 μl ligase (1.5 U) was added and the ligation run for 2 h, before analysing the pseudorotaxane on a 2% agarose gel in 0.5 × TAE. Release oligo 105-Insert (10 equiv.) and, 15 min later, 20 equiv. of release oligo Endf2-Insert were added and the ligation continued.

Dethreading. The gap-ring (2 equiv.) and the DNA rod (1 equiv.) in 20 μl of 1 × ligase buffer were threaded at room temperature overnight and then cooled to 15 °C for 1 h. A solution of 2.5 equiv. of stopper in 14 μl of 1 × ligase buffer was added, so that the final concentrations were 0.2 μM gap-ring, 0.1 μM DNA rod and 0.25 μM stopper. After hybridizing for 30 min at 15 °C, 0.3 μl ligase (1.5 U) was added and the ligation left to proceed for 2 h. The formation of the pseudorotaxane was verified by separating 4 μl of the sample on agarose gel. The remaining sample was cooled to 4 °C and 5 μl of the solution were taken out (0 time point). A volume of 1 μl of a 50 μM solution of Insert105 (20 equiv. with respect to the DNA rod) was added. After the indicated time points, samples of 5 μl were taken out, diluted with 1 μl glycerol/H$_2$O (1:1), and immediately frozen in liquid nitrogen. Immediately before gel electrophoresis, all samples were quick-thawed at 4 °C, and separated on a 2.2% agarose gel at 4 °C.

Atomic force microscopy. AFM images were taken on a Veeco Dimension 3100 AFM with a Nanoscope IIIa controller in tapping mode. Imaging was performed both in buffer or in air. A volume of 30 μl of a solution of 0.1 mg polyornithin (P3655, Sigma Aldrich) in 1 ml TAE-Mg buffer, the same as was used for AFM imaging (40 mM Tris/acetic acid pH 7.5, 2.5 mM EDTA, 12.5 mM MgCl$_2$), was applied on freshly cleaved mica (muscovite grade, Plano) and incubated for ∼2 min. The surface was rinsed with milli-Q water and dried with a stream of nitrogen. For imaging, the respective samples were diluted with TAE-Mg buffer to a final concentration of between 2 and 5 nM. A volume of 4 μl of this solution was applied on the pre-treated mica surface and incubated for a minute. For dry imaging, the TAE-Mg buffer was briefly washed off with a few millilitres of milli-Q water and immediately dried with a stream of nitrogen. These samples could be stored for weeks at room temperature without any signs of decomposition of the DNA. For liquid-mode imaging the sample was not washed and dried. A volume of 30 μl of TAE-Mg buffer was added both to the sample and on the probe holder. Liquid-mode imaging resulted in better contrasted images than those obtained in dry-mode imaging, but the tips wore off more quickly. Liquid mode: a Veeco fluid cell (DTFML-DD) was used with Veeco DNP-S tips (0.12–0.58 N m^{-1}) in tapping mode. The amplitude setpoint was set to 300 mV and typical resonance frequencies of the cantilevers were between 19 and 20 kHz. Scanning frequencies were between 1 and 2 Hz. In the dry mode, ACT probes (25–75 N m^{-1}) from APP Nano were used for imaging in air. The typical resonance frequencies of the cantilevers were between 300 and 400 kHz. The amplitude setpoint was set to 0.3 V, and scanning frequencies were between 0.5 and 2 Hz. Before imaging, all the AFM probes were irradiated with a UV handlamp for 2–12 h from a distance of 1–2 cm. AFM raw data were processed with Nanoscope(R) 5.31 software (Veeco), and height profiles were obtained with the freeware program WSxM (Nanotec[47]).

Fluorescence spectroscopy. The HPLC-purified Cy3-BHQ2-labelled pseudorotaxane (80 μl, ∼50 nM) in 1 × DNA buffer was irradiated at 548 nm at 20 °C. Fluorescence emission was measured 10 times at 600 nm for 500 ms. The sample was treated with SO (0.5 μl, 100 μM) and the fluorescence measured after 5 and 60 min. Then RO (0.5 μl, 100 μM) was added to the sample, and after 5 min the emission measured again. The values of ten measurements were averaged and the standard deviations calculated.

References

1. Arico, F. *et al.* Templated synthesis of interlocked molecules. *Top. Curr. Chem.* **249,** 203–259 (2005).
2. Schalley, C. A., Beizai, K. & Vögtle, F. On the way to rotaxane-based molecular motors: studies in molecular mobility and topological chirality. *Acc. Chem. Res.* **34,** 465–476 (2001).
3. Stoddart, J. F. The chemistry of the mechanical bond. *Chem. Soc. Rev.* **38,** 1802–1820 (2009).
4. Fernandes, A. *et al.* Rotaxane-based propeptides: protection and enzymatic release of a bioactive pentapeptide. *Angew. Chem. Int. Ed.* **48,** 6443–6447 (2009).
5. Gassensmith, J. J. *et al.* Self-assembly of fluorescent inclusion complexes in competitive media including the interior of living cells. *J. Am. Chem. Soc.* **129,** 15054–15059 (2007).
6. Cacialli, F. *et al.* Cyclodextrin-threaded conjugated polyrotaxanes as insulated molecular wires with reduced interstrand interactions. *Nature Mater.* **1,** 160–164 (2002).
7. Kay, E. R., Leigh, D. A. & Zerbetto, F. Synthetic molecular motors and mechanical machines. *Angew. Chem. Int. Ed.* **46,** 72–191 (2007).
8. Amabilino, D. B. & Stoddart, J. F. Interlocked and intertwined structures and superstructures. *Chem. Rev.* **95,** 2725–2828 (1995).
9. Balzani, V., Credi, A. & Venturi, M. Light powered molecular machines. *Chem. Soc. Rev.* **38,** 1542–1550 (2009).
10. Green, J. E. *et al.* A 160-kilobit molecular electronic memory patterned at 10(11) bits per square centimetre. *Nature* **445,** 414–417 (2007).

11. Wang, Q. C., Qu, D. H., Ren, J., Chen, K. & Tian, H. A lockable light-driven molecular shuttle with a fluorescent signal. *Angew. Chem. Int. Ed.* **43,** 2661–2665 (2004).

12. Nguyen, T. D. *et al.* A reversible molecular valve. *Proc. Natl Acad. Sci. USA* **102,** 10029–10034 (2005).

13. Berna, J. *et al.* Macroscopic transport by synthetic molecular machines. *Nature Mater.* **4,** 704–710 (2005).

14. Seeman, N. C. An overview of structural DNA nanotechnology. *Mol. Biotechnol.* **37,** 246–257 (2007).

15. Heckel, A. & Famulok, M. Building objects from nucleic acids for a nanometer world. *Biochimie* **90,** 1096–1107 (2008).

16. Feldkamp, U. & Niemeyer, C. M. Rational design of DNA nanoarchitectures. *Angew. Chem. Int. Ed.* **45,** 1856–1876 (2006).

17. Rothemund, P. W. K. Folding DNA to create nanoscale shapes and patterns. *Nature* **440,** 297–302 (2006).

18. Rothemund, P. W. K., Papadakis, N. & Winfree, E. Algorithmic self-assembly of DNA Sierpinski triangles. *PLoS Biol.* **2,** e424 (2004).

19. Mao, C. D., LaBean, T. H., Reif, J. H. & Seeman, N. C. Logical computation using algorithmic self-assembly of DNA triple-crossover molecules. *Nature* **407,** 493–496 (2000).

20. Saghatelian, A., Völcker, N. H., Guckian, K. M., Lin, V. S. Y. & Ghadiri, M. R. DNA-based photonic logic gates: AND, NAND and INHIBIT. *J. Am. Chem. Soc.* **125,** 346–347 (2003).

21. Miyoshi, D., Inoue, M. & Sugimoto, N. DNA logic gates based on structural polymorphism of telomere DNA molecules responding to chemical input signals. *Angew. Chem. Int. Ed.* **45,** 7716–7719 (2006).

22. Winfree, E., Furong, L., Wenzler, L. A. & Seeman, N. C. Design and self-assembly of two-dimensional DNA crystals. *Nature* **394,** 539–544 (1998).

23. Goodman, R. P. *et al.* Rapid chiral assembly of rigid DNA building blocks for molecular nanofabrication. *Science* **310,** 1661–1665 (2005).

24. Yin, P., Choi, H. M. T., Calvert, C. R. & Pierce, N. A. Programming biomolecular self-assembly pathways. *Nature* **451,** 318–322 (2008).

25. Bath, J. & Turberfield, A. J. DNA nanomachines. *Nature Nanotech.* **2,** 275–284 (2007).

26. Simmel, F. C. & Dittmer, W. U. DNA nanodevices. *Small* **1,** 284–299 (2005).

27. Schliwa, M. *Molecular Motors* (Wiley-VCH, 2003).

28. Yan, H., Zhang, X., Shen, Z. & Seeman, N. C. A robust DNA mechanical device controlled by hybridization topology. *Nature* **415,** 62–65 (2002).

29. Shin, Y. S. & Pierce, N. A. A synthetic DNA walker for molecular transport. *J. Am. Chem. Soc.* **126,** 10834–10835 (2004).

30. Omabegho, T., Sha, R. & Seeman, N. C. A bipedal DNA brownian motor with coordinated legs. *Science* **324,** 67–71 (2009).

31. Ryan, K. & Kool, E. T. Triplex-directed self-assembly of an artificial sliding clamp on duplex DNA. *Chem. Biol.* **5,** 59–67 (1998).

32. Weizmann, Y., Braunschweig, A. B., Wilner, O. I., Cheglakov, Z. & Willner, I. A polycatenated DNA scaffold for the one-step assembly of hierarchical nanostructures. *Proc. Natl Acad. Sci. USA* **105,** 5289–5294 (2008).

33. Mayer, G., Ackermann, D., Kuhn, N. & Famulok, M. Construction of DNA architectures with RNA hairpins. *Angew. Chem. Int. Ed.* **47,** 971–973 (2008).

34. Rasched, G. *et al.* DNA minicircles with gaps for versatile functionalization. *Angew. Chem. Int. Ed.* **47,** 967–970 (2008).

35. Schmidt, T. L. *et al.* Polyamide struts for DNA architectures. *Angew. Chem. Int. Ed.* **46,** 4382–4384 (2007).

36. Han, W., Dlakic, M., Zhu, Y. J., Lindsay, S. M. & Harrington, R. E. Strained DNA is kinked by low concentrations of Zn^{2+}. *Proc. Natl Acad. Sci. USA* **94,** 10565–10570 (1997).

37. Wimberly, B. T. *et al.* Structure of the 30S ribosomal subunit. *Nature* **407,** 327–339 (2000).

38. Raymo, F. M. & Stoddart, J. F. Slippage—a simple and efficient way to self-assemble [*n*]rotaxanes. *Pure Appl. Chem.* **69,** 1987–1997 (1997).

39. Ashton, P. R. *et al.* Rotaxane or pseudorotaxane? That is the question! *J. Am. Chem. Soc.* **120,** 2297–2307 (1998).

40. Clegg, R. M. *et al.* Fluorescence resonance energy transfer analysis of the structure of the four-way DNA junction. *Biochemistry* **31,** 4846–4856 (1992).

41. Mao, C., Sun, W. & Seeman, N. C. Designed two-dimensional DNA Holliday junction arrays visualized by atomic force microscopy. *J. Am. Chem. Soc.* **121,** 5437–5443 (1999).

42. Eichman, B. F., Vargason, J. M., Moores, B. H. M. & Ho, P. S. The Holliday junction in an inverted repeat DNA sequence: sequence effects on the structure of four-way junctions. *Proc. Natl Acad. Sci. USA* **97,** 3971–3976 (2000).

43. Sha, R., Liu, F. & Seeman, N. C. Atomic force microscopic measurement of the interdomain angle in symmetric Holliday junctions. *Biochemistry* **41,** 5950–5955 (2002).

44. Dietz, H., Douglas, S. M. & Shih, W. M. Folding DNA into twisted and curved nanoscale shapes. *Science* **325,** 725–730 (2009).

45. Raymo, F. M., Houk, K. N. & Stoddart, J. F. The mechanism of the slippage approach to rotaxanes. Origin of the 'all-or-nothing' substituent effect. *J. Am. Chem. Soc.* **120,** 9318–9322 (1998).

46. Bowman, G. D., Goedken, E. R., Kazmirski, S. L., O'Donnell, M. & Kuriyan, J. DNA polymerase clamp loaders and DNA recognition. *FEBS Lett.* **579,** 863–867 (2005).

47. Horcas, R. *et al.* WSXM: a software for scanning probe microscopy and a tool for nanotechnology. *Rev. Sci. Instrum.* **78,** 013705 (2007).

Acknowledgements

Author contributions

D.A. performed and designed, with M.F., most of the included studies. C.S.P. performed the dethreading experiments. J.H. provided conceptual input. T.L.S. performed the AFM studies, assisted by A.H. M.F. supervised the research project and assisted in the experimental design. All authors discussed the experimental results. D.A., J.H. and M.F. wrote the manuscript.

Additional information

The authors declare no competing financial interests. Supplementary information accompanies this paper at www.nature.com/naturenanotechnology. Reprints and permission information is available online at http://npg.nature.com/reprintsandpermissions/. Correspondence and requests for materials should be addressed to M.F.